Neural Computing and Applications
https://doi.org/10.1007/s00521-023-08909-y

ORIGINAL ARTICLE

Diagnosis of breast cancer based on hybrid features extraction in dynamic contrast enhanced magnetic resonance imaging

Ali M. Hasan[1] · Hadeel K. Aljobouri[2] · Noor K. N. Al-Waely[3] · Rabha W. Ibrahim[4,5,6] · Hamid A. Jalab[4,7] · Farid Meziane[8]

Received: 9 January 2023 / Accepted: 21 July 2023

Abstract
Breast cancer develops in breast cells. It is the most common type of cancer in women and the second most lethal disease after lung cancer. The presence of breast masses is an important symptom for detecting breast cancer in its early stages. This study proposes a hybrid features extraction method to improve the automatic detection of breast cancer by combining three feature extraction methods: Kinetic Features, convolutional neural network deep learning features, and the newly proposed Quantum Chebyshev polynomials model. The long short-term memory model is used as a classifier in this study to detect breast cancer automatically, which could reduce human errors in the diagnosis process. The experimental results using a large publicly available dataset achieved a detection accuracy of 99.50% for hybrid features in post-contrast 2, potentially reducing human errors in the diagnosis process.

Keywords Kinetic features · CNN · Quantum Chebyshev polynomials · LSTM · DCE-MRI

1 Introduction

Breast cancer occurs in the breast tissue and is one of the most common types of cancer in women around the world. For the last two decades, the incidence rate of new cancer cases in Iraq has been increasing. The age-standardized incidence rates (ASIRs) in 2019 were more than double the rate estimated in 2000. There was particularly a significant increase trend for breast cancer incidence during the period of 2000–2019 when the study was conducted [2, 12, 35]. The earlier the diagnosis of breast cancer is performed, and the better the outcomes are in the long-term. Unfortunately,

✉ Ali M. Hasan
alialwaeli@nahrainuniv.edu.iq

Hadeel K. Aljobouri
hadeel.k.aljobouri@nahrainuniv.edu.iq

Noor K. N. Al-Waely
noor83kadhem@nahrainuniv.edu.iq

Rabha W. Ibrahim
rabha@alayen.edu.iq; rabhawaell.ibrahim@lau.edu.lb; rabhawaell.ibrahim@neu.edu.tr

Hamid A. Jalab
hamidjalab@um.edu.my

Farid Meziane
f.meziane@derby.ac.uk

[1] Physiology and Medical Physics Department, College of Medicine, Al-Nahrain University, Kadhimiya, Baghdad, Iraq

[2] Biomedical Engineering Department, College of Engineering, Al-Nahrain University, Baghdad, Iraq

[3] General Surgery Department, College of Medicine, Al-Nahrain University, Kadhimiya, Baghdad, Iraq

[4] Information and Communication Technology Research Group, Scientific Research Center, Al-Ayen University, Nile Street, Thi-Qar 64001, Iraq

[5] Department of Computer Science and Mathematics, Lebanese American University, Beirut 1102 2801, Lebanon

[6] Mathematics Research Center, Department of Mathematics, Near East University, Near East Boulevard, 99138 Nicosia/ Mersin 10, Turkey

[7] Faculty of Computer Science and Information Technology, University of Malaya, 50603 Kuala Lumpur, Malaysia

[8] Data Science Research Centre, School of Computing and Engineering, University of Derby, Derby, UK

Published online: 30 August 2023

there are many cases of the disease in advanced stages in developing countries. This reduces dramatically patients' survival rates. Locally Advanced Breast Cancer (LABC) can be defined as a multi degree disease that involves several parts of the breast tissue and the wall of the chest [20]. It mostly occurs in the ducts of milk or associated lobules. The most common types of breast cancer are Ductal Carcinoma in Situ (DCIS), Infiltrating Ductal Carcinoma (IDC), Lobular Carcinoma in Situ (LCIS), and Infiltrating Lobular Carcinoma (ILC) [30]. However, Breast cancer is a curable disease, and survivors can have a life similar to that of healthy people.

Imaging is one of the many methods used first to detect a breast mass, and there are many medical imaging techniques available. Mammography is often used for the screening of a mass and is not challenged by bone structures or blood vessels. In fact, mammography is one of the effective tools used for screening breast cancer. Screening is one of the most effective methods to detect cancer in early stages, and mammography has a strong contribution to the screening process. Screening is recommended in clinical practice and guidelines and can contribute to increasing the survival rates by 5 years. However, mammography has limitations when screening dense tissue as the sensitivity and specificity decrease when compared to other imaging modalities [5, 15].

Ultrasound is a medical imaging that is also used for breast mass detection and evaluation; it is a low-cost modality that is often used for screening. However, it has less sensitivity than other available imaging techniques and requires an experienced radiologist. Scanning by Computed Tomography (CT) is also used for tumor detection in the breast [3, 31]. There are some drawbacks related to the use of CT that include the radiation risks, the low sensitivity of the modality and the use of the system is relatively expensive. Positron Emission Tomography (PET) is one of the few imaging modalities that provide good functional assessment of the human body in general and can provide imaging of breast masses. Unfortunately, PET is using ionized radiation and has radiation risks [34]. Scanning with Magnetic Resonance Imaging (MRI) has proved to be effective in obtaining small details in a tissue, thus is being used to evaluate women with high risk of developing breast mass. MRI is providing means for early diagnosis and was found to be capable of enhancing the identification of breast cancer and has better sensitivity compared to mammography when it comes to patients with dense breast tissue [9]. One of the important parts affecting the image is the Radiofrequency (RF) coil that transmits and receives radiofrequency as depicted in Fig. 1. Tissue under examination may go inside the coil and these types of coils are called volume coils. If the tissue being examined is placed closely under the coil, the type of the coil in this case is a surface coil [16]. Modern MRI scanners generate various sequences that can be classified based on the appearance of tissues. The most popular MRI sequences are T1 and T2. T1 is known as longitudinal relaxation, which varies depending on the tissue type.

T2 is the transverse relaxation and occurs when the spins relax in the transverse plane. When the magnetic field travels through the tissue, it will start to possess some inhomogeneity. Therefore, some spins fall out of synchronization. Desynchronizations happen in this case due to the inhomogeneity in the magnetic field resulting in a T2 signal. Tissue with long T1 signal appears dark in the image as they emit less signal and vice versa. However, long T2 signal reflects dark tissue in the images [17, 40].

There are some other means of detecting cancers other than imaging modalities, and this includes clinical examination and palpation, pathological examination through fine needle aspiration or biopsy, histopathological evaluation which can potentially help identify cancer type, and biomarkers such as the cancer cells DNA and mRNA [23]. The tumor size can be determined by imaging, but this could be challenging when a small size tumor is under examination, subsequently resulting in difficulties to identify margins before surgical removal [30].

Dynamic Contrast Enhanced Magnetic Resonance Imaging (DCE-MRI) is routinely used for early diagnoses of breast cancer staging. The DCE-MRI time-signal intensity curve (TIC) reflects the hemodynamic characteristics of a specific lesion. The TIC is obtained through repeated MRI scans following the injection of a contrast agent; a qualified TIC typically takes 12 min to complete the scans. The output signal over a selected time interval can be described using kinetic curves for obtaining quantitative data of a Region of Interest (ROI). To analyze TICs from breast DCE-MRI, the circular ROI must be placed on the part of lesion that has fastest enhancement with fastest washout, or the most worrisome part. There are no uniform criteria for interpreting the kinetic curve. Some authors are

Fig. 1 Philips breast coil of an MRI machine [16]

more concerned with the shape of the TIC under DCE-MRI, whereas others are more concerned with the enhancement threshold values of malignancy [36].

During repetitive performance, semi-quantitative development kinetic features are often used to progress specificity for detecting malignancy. There is an initial peak development phase, and the existence of a delayed phase washout, as defined by the American College of Radiology (ACR) Breast Imaging Reporting and Data System (BI-RADS) Breast MRI Atlas [32, 44]. So, the curves are divided into different types, as shown in Fig. 2 [29]. Type I denotes a developing form that indicates a steady increase in the signal strength over time. The Type II curve exhibits a plateau pattern with an initial uptake of contrast molecules followed by a plateau phase, which is symptomatic of a malignant tumor. The Type III curve is a washout pattern with an initial quick uptake and a subsequent decrease in signal enhancement that is highly predictive of malignancy [29].

In order to provide more diagnostic information and decrease unnecessary breast biopsies, this study uses a kinetic model with DCE-MRI combined with deep and textural features that were derived from breast lesions.

2 Related works

Recently, many studies have taken advantage of the vital function of kinetic models to enhance breast lesion diagnosis by precisely differentiating benign and malignant lesions. A CNN model was developed by Chen et al. [6] on the basis of DCE-MRI to define and predict the malignancy of breast lesions using a training/validation dataset of, 6165 slices from 364 patients (234 malignant, 130 benign). The accuracy, sensitivity, and specificity of the slice-based technique were 90.3%, 96.2%, and 79.0%, respectively, while the area under the Receiver Operating Characteristic (ROC) curve for breast cancer prediction was 0.955. Peng et al. [38] examined the abilities of Deep Learning (DL)

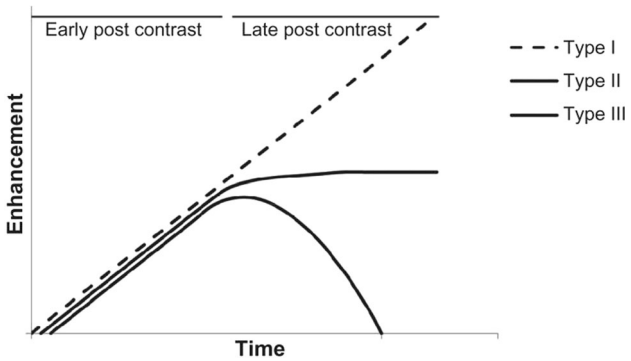

Fig. 2 Different types of kinetic curves from DCE-MRI [29]

and Radiomics Analysis (RA) to predict pathological Complete Response (pCR) to Neo Adjuvant Chemotherapy (NAC) in breast cancer based on pre-treatment DCE-MRI. This retrospective study included 356 breast cancer patients who had DCE-MRI prior to NAC and surgery after NAC. DCE-MRI was used to derive the image characteristics and kinetic parameters of malignancies. By incorporating kinetic parameters or molecular data into image-only Linear Discriminant Analysis (LDA) and CNN models, the image-based RA and DL models were developed. The image-kinetic-molecular DL model's 0.83 area under the ROC curve was higher than that of the image-kinetic and image-molecular DL and RA models. Using Fully Convolutional Networks, Zhang et al. [47] proposed a framework for breast tumor segmentation (FCN) based on Mask-guided Hierarchical Learning (MHL). In order to remove distracting information from the input DCE-MR images, they first created an FCN model to produce a 3D breast mask as the ROI for each image. Then, to do coarse-to-fine segmentation for breast cancers, they created a two-stage FCN model. To address the class-imbalance issue, they specifically suggested a Dice-Sensitivity-like loss function and a reinforcement sampling approach. A mean Dice Similarity Coefficient (DSC) of 0.72, which is equivalent to mutual DSC between expert radiologists, was obtained when they verified the MHL approach on 272 cases.

Piantadosi et al. [39] introduced the Breast Lesion Automatic Detection and Diagnosis System (BLADeS), and a comprehensive fully automated breast CAD system designed to assist the radiologist with patient diagnosis. They suggested a hierarchical architecture with modules for breast segmentation, attenuating motion artifacts, localizing lesions, and, finally, classifying lesions according on their malignancy. To achieve a valid comparison, performance was assessed on 42 individuals with histopathologically identified lesions. Piantadosi et al. [39] used deep learning to automate breast lesion segmentation in DCE-MRI, based on past learned by training the proposed architecture on images taken at very particular time intervals. To do this, they suggested the Three Time Points (3TP) U-Net, a U-Shaped deep convolutional neural network that may be used to enhance lesion segmentation results by utilizing the well-known 3TP technique. The proposed technique enhances the dynamic course of the contrast agent while minimizing the effect of noise, which increases the lesion segmentation effectiveness. In addition, the results have shown that deep-based methods always outperform non-deep ones, with the introduced 3TP U-Net performing better in terms of median DSC. Jing et al. [26] proposed a computer-aided diagnosis method based on morphological features and kinetic curve assessment. To determine the malignancy of breast lesions in

MRI images, morphological features should be considered first, followed by others such as temporal data in dynamic contrast enhanced MRI sequences. A 2D CNN and a LSTM network were utilized to extract morphological characteristics and kinetic information, respectively, in this technique. The extracted features from these two methods were then combined to achieve a mean AUC of 83% in classifying a total of 173 pathologically confirmed MRI breast slices (109 and 64 MRI slices were benign and malignant, respectively). Hu et al. [18] proposed an automated method for improving the clinical diagnosis of pathological breast using multiparametric MRI. Individual features from DCE-MRI and T2w sequences were extracted using the pretrained CNN. The combined features significantly improved diagnostic performance, with an AUC of 87% for distinguishing benign from malignant lesions. From previous studies, the existing models for distinguishing innocuous benign disorders from life threatening malignant breast cancers rely essentially on deep features or temporal kinetic features. Therefore, combining the handcrafted features that are extracted from the multitemporal images at various time points, with the deep and kinetic features will further improve the performance of breast cancer diagnosis.

The motivation for this study is to develop and validate a very powerful and reliable automated system offering possibilities for differentiating malignant from benign breast lesions by combining Quantum Chebyshev polynomials (QCHPs), DL, and kinetic features from DCE-MRI. Our contribution can be summarized as follows:

1. The new proposed QCHPs method which is used as a feature extractor for image classification tasks.
2. Effective use of multiple breast cancer characteristics features that may improve the detection of breast malignancy with better precision, as well as, reducing unnecessary biopsies.

The remaining sections of this paper are organized as follows; Sect. 3 provides the details of the proposed model for classifying breast DCE-MRI sequences; Sect. 4 presents the experimental results; and finally, the conclusions are given in Sect. 5.

3 Material and method

In this study, utilization of kinetic, QCHPs, and deep features of DCE-MRI of the breast are used to improve the diagnosis process by reducing unnecessary follow-ups or biopsies for many breast masses.

The proposed study includes four stages. The first stage is the data collection, preprocessing, feature extraction, combining features and classification.

The preprocessing is to enhance the quality of input images; the feature extraction, three methods for the feature extraction are applied: Kinetic features; B. CNN deep learning features and the hand crafted (QCHPs) features. The combining features strategy of all extracted features to generate the feature vector for the classification stage. The final stage is the classification process, in which LSTM classifier is utilized. The flow process is illustrated in Fig. 3.

The proposed model aims to quickly identify patients with pathological breasts and classify them into benign or malignant. The kinetic features are determined after implementing TIC analysis using the Radiant Software by experienced radiologists. The proposed model comprises three main stages namely: (i) DCE-MRI slices preprocessing; (ii) feature extraction and finally (iii) an LSTM network is used to classify these features into benign and malignant.

3.1 Breast DCE-MRI dataset

The breast DCE-MRI dataset used in this study was downloaded from Duke University Medical Center, and acquired from January 1, 2000 to March 23, 2014 [41]. A total number of 600 patients with histopathological confirmation were selected from 922 patients for the present study and excluded patients with previous surgical excision, or chemotherapy, or radiotherapy, invisible lesions, and lesions without final pathology results. The final dataset used in this study includes 300 DCE-MRI sequences of histopathology proven malignant patients and 300 DCE-MRI sequences of histopathology proven benign patients. All breast DCE-MRI examinations were performed using 1.5 T and 3 T systems (GE medical system and Siemens) using breast array coil with four dedicated channels. Each DCE-MRI sequence comprised a pre-contrast T1 weighted scan acquired prior to multiple T1 weighted post-contrast scans with contrast injection. All patients had a single lesion in either left or right breast and confirmed in both pathologic and imaging studies. Additionally, the region of interest (ROI) around the breast lesion was outlined manually by a consultant radiologist to confirm the provided annotations of the downloaded dataset.

3.2 DCE-MRI breast image preprocessing

Artifacts in MRI can be caused by the scanner hardware or by the patient's interaction with the hardware. Artifacts in MRI scans may be confused with a pathology or just reduce the quality of examinations and resulting in mimic pathologies and improper diagnoses [27]. These artifacts can be categorized into three main sources: physiologic

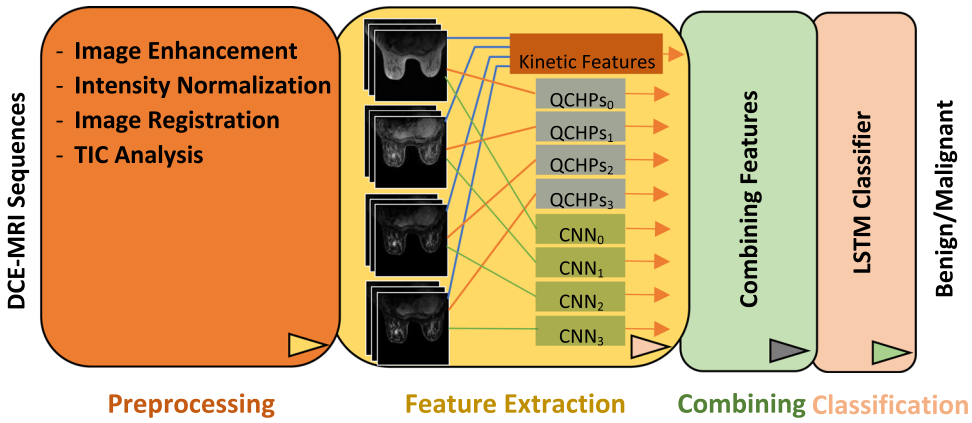

Fig. 3 Flow process for MRI classification

artifacts, inherent physical artifacts, and hardware and software artifacts. Physiologic artifacts are generated from patient movement, including breathing, heartbeat, and blood flow. This type of artifacts typically appears as blurring or ghosting, while inherent physical artifacts, also known as chemical-shift artifacts, occur during the frequency encoding of the MRI process. This makes the edges of the anatomy appear as a black or bright band and may be diagnosed as pathological. Therefore, several methods have been proposed to remove artifacts and improve the diagnostic quality [42]. Additionally, major cons of MRI compared to other medical imaging modalities are the fact that its intensities are not standardized and varied between the same and consecutive MRI slices due to MRI scanners. Moreover, acquiring MRI data from different scanners at different sites produce variances in the dynamic intensity range of the MRI slices even when they use identical acquisition protocols. Furthermore, when different manufacturers and scanner-models are used, bias field and different pulse sequence parameters can cause the variation in the intensity of MRI scan [10, 14]. Therefore, all breast DCE-MRI were enhanced by Gaussian filter method and normalized by the histogram normalization method to eliminate intensity variations from any postprocessing steps [10, 11, 14]. In addition, all breast DCE-MRI scans were registered to the same spatial resolution by scaling using bilinear interpolation because the dataset was captured using a variety of imaging devices with varying pixel spacing and spatial resolutions [49]. Then, to determine and quantify the tumor vascularity of the breast, the DCE-MRI was analyzed to reflect the hemodynamic characteristics of breast lesions, by drawing manually the TIC patterns using Radiant software. An experienced radiologist with 10 years of experience who was blinded to patient clinical information placed a circular ROI with diameters in the range of 20–30 pixels, along the edge of the suspicious lesion area that exhibits strongest enhancement in all sequences during and after intravenous contrast agent injection [45]. When selecting the ROI, the non-enhanced regions such as the edge of the lesions, bleeding, necrosis, cystic degeneration, and blood vessels in the tumor are avoided as much as possible [43, 45, 48, 49]. Then, the TICs are usually obtained from a selected ROI of each examination and classified subjectively into three patterns (persistent, plateau, and washout). The TIC shape gives an endpoint indication for diagnosing breast lesions, but it is not used as a final decision for determining the malignance of breast lesions [28].

3.3 Feature extraction

A. Kinetic features

Following the extraction of the TIC pattern of the lesion area, the quantitative analysis of the delayed phase of TIC was performed to categorized it into three types (persistent, plateau, and washout) based on Eq. (1) [33, 46].

$$SI_{\text{Slope}} = \frac{(SI_{\text{tail}} - SI_{\text{mean}})}{SI_{\text{mean}}} \times 100\% \quad (1)$$

where SI_{mean} represents the mean values of the first and second post-contrast time points. SI_{tail} indicates the signal intensity of the last time point. Then, the TIC pattern is classified as persistent when SI_{Slope} is greater than 10%, as a washout when SI_{Slope} is less than $-$ 10%, and otherwise, it is considered as a plateau.

Moreover, the kinetic curve can be used to compute a number of fundamental characteristics derived from the TIC pattern.

- The mean curve measure is determined by Eq. (2) [33, 46].

$$MSI = \text{Max}(SI_{i+1} - SI_i) \quad (2)$$

  where SI_i and SI_{i+1} represent the signal intensity of the former and latter time points respectively. i denotes the time points, and ranges between 0 and 4 in this study.
- The initial percentage of enhancement is determined by Eq. (3) [33, 46].

$$E_{\text{Initial}} = \frac{(SI_1 - SI_0)}{SI_0} \times 100\% \quad (3)$$

where SI_1 and SI_0 represent the first post-contrast and pre-contrast time points respectively.

- The percentage of peak enhancement is determined by Eq. (4) [33, 46].

$$E_{\text{Peak}} = \frac{(SI_{\text{Peak}} - SI_0)}{SI_0} \times 100\% \quad (4)$$

where SI_{Peak} indicates the peak value of the signal intensity at any time point.

- The early signal enhancement ratio is determined by Eq. (5) [33, 46].

$$ESER = \frac{(SI_1 - SI_0)}{(SI_2 - SI_0)} \times 100\% \quad (5)$$

where SI_2 represents the second post-contrast time point.

- The second enhancement percentage is determined by Eq. (6) [33, 46].

$$SEP = \frac{(SI_2 - SI_0)}{SI_0} \times 100\% \quad (6)$$

- Finally, the gradient (θ) is the slope of the tangent that touches the signal intensity at each time point. It is calculated by dividing the vertical change by the horizontal change between each pair of successive signal intensity time points. θ is determined by Eq. (7).

$$\theta = \tan^{-1} \frac{(SI_{i+1} - SI_i)}{(t_{i+1} - t_i)} \quad (7)$$

where θ is positive when the intensity curve increases and negative when it decreases.

Four features are extracted by the gradient method from kinetic curve of breast lesions. Consequently, ten kinetic features are extracted from every breast DCE-MRI, which provide a quantitative basis for distinguishing between benign and malignant breast lesions.

B. CNN architecture for feature extraction

Even though the kinetic features are designed based on expert knowledge, they have a very high sensitivity and a relatively low specificity for diagnosing breast lesions [15, 45]. The low specificity indicates that there are common characteristics shared by benign and malignant lesions. This leads to produce a high number of false-positive cases and unnecessary biopsies [7]. Therefore, to efficiently extract more features for diagnosing breast lesions accurately, a learning-based technique is used to learn more features with high specificity using a CNN method as it was applied successfully in many medical applications [15, 18, 19, 49].

The procedure for the extraction of deep features from breast DCE-MRI sequences (t_0, t_1, t_2, and t_3 respectively) includes cropping breast lesions manually by an experienced radiologist prior to the implementation of the CNN. The cropping is based on the maximum dimension of each breast lesion. The image rescaling is avoided because of the distortion of precious high-frequency details. So, a margin of zero pixels around the cropped lesion image was added to unify images prior to implementing the CNN. All cropped images were standardized to 98 × 98 pixels as required by the CNN architecture. The used CNN consists of a set of convolution layers, pooling layers, an activation function, and a fully connected layer. These layers are used to transform the DCE-MRI slices into the desired output after training [15]. Each convolution layer includes a set of kernel filters which are slid across the DCE-MRI slice by shifting and multiplying from one position to another to extract certain features. This procedure is called stride and a stride refers to the number of pixels that the kernel filter will skip. Therefore, the spatial dimensions of the output volume after every layer decrease significantly. Then, the output of convoluting kernel filters is rectified by eliminating the negative numbers from the feature maps by using the ReLU activation function and passed through pooling layer for down sampling. Consequently, a batch normalization layer is used to normalize feature maps and regularize the training process of the CNN. Finally, the weights of CNN improve and subsequently the error function decreases by using the gradient-based optimization algorithm [13].

The proposed structure of extracting deep features (DF) from breast DCE-MRI sequence is illustrated in Fig. 4. The same CNN is used to extract DF from pre-contrast at t_0 and post-contrast (t_1, t_2, and t_3 respectively), as illustrated in Fig. 5. Consequently, two DFs are extracted from every time phase of the MRI slice.

C. Image feature extraction based on Quantum Chebyshev polynomials (QCHPs)

This study aims to explore a novel feature extraction model based on QCHPs. The concepts of fractional calculus are mentioned as important tools for investigating studies of discontinuity or local continuity (discrete) [1, 21, 24], while the quantum calculus represent suitable roles to generalize many concepts in mathematics, engineering and physics [22]. In this effort, a q-calculus has been proposed to generalize the Chebyshev polynomial and formulate it in a convolution linear operator.

The q-exponential $e_q(\chi)$ is formulated by Eq. (8).

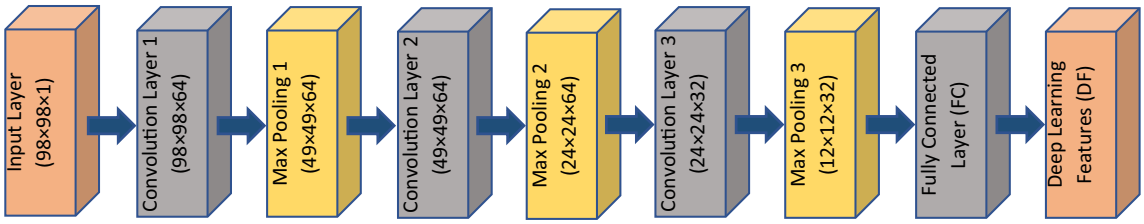

Fig. 4 Structure of DF extraction

Fig. 5 Proposed model for DF extraction from DCE-MRI

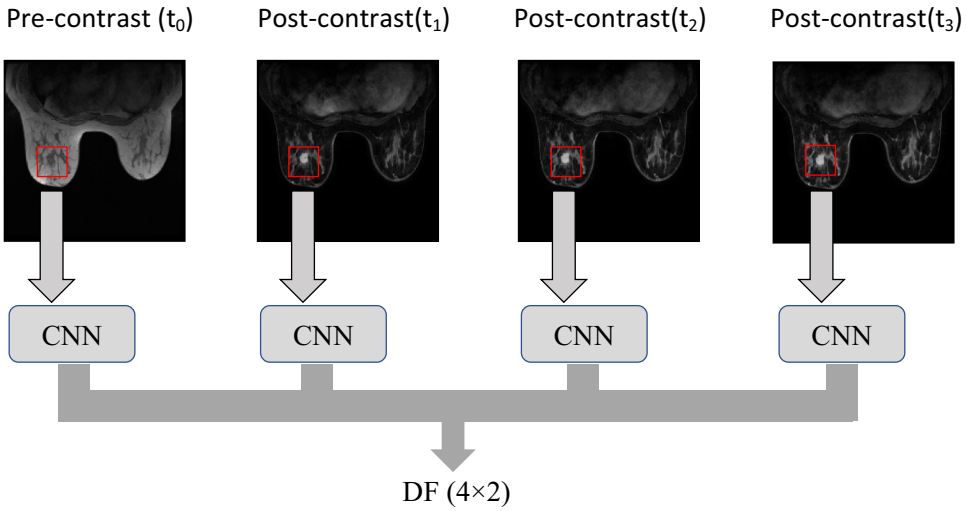

$$
\begin{aligned}
e_q(\chi) &= \sum_{n=0}^{\infty} \frac{\chi^n}{[n]_q!} = \sum_{n=0}^{\infty} \frac{\chi^n (1-q)^n}{(q;q)_n} \\
&= \sum_{n=0}^{\infty} \chi^n \frac{(1-q)^n}{(1-q^n)(1-q^{n-1})\cdots(1-q)}, [n]_q \\
&= \frac{q^n - 1}{q-1}
\end{aligned} \tag{8}
$$

where $[n]_q!$ is the q-factorial; $(q;q)_n$ is the q-Pochhammer expression and is formulated by Eq. (9).

$$
(q;q)_n = (1-q^n)(1-q^{n-1})\cdots(1-q) \tag{9}
$$

The Chebyshe polynomials $\mathcal{T}_n() = \cos(n \times \arccos())$ of the first kind are obtained from the recurrence relation.

$$
\begin{aligned}
T_0(\chi) &= 1 \\
T_1(\chi) &= \chi \\
T_{n+1}(\chi) &= 2\chi T_n(\chi) - T_{n-1}(\chi).
\end{aligned} \tag{10}
$$

The ordinary generating function for T_n is

$$
\sum_{n=0}^{\infty} T_n(\chi) t^n = \frac{1 - t\chi}{1 - 2t\chi + t^2} \tag{11}
$$

Note that

$$
T_n(\chi) = n \sum_{k=0}^{n} (-2)^k \frac{(n+k-1)!}{(n-k)!(2k)!} (1-\chi)^k, n > 0. \tag{12}
$$

Moreover, the exponential generating function is

$$
\begin{aligned}
\sum_{n=0}^{\infty} T_n(\chi) \frac{t^n}{n!} &= \frac{1}{2}\left(e^{t\left(\chi - \sqrt{\chi^2-1}\right)} + e^{t\left(\chi + \sqrt{\chi^2-1}\right)}\right) \\
&= e^{t\chi} \cosh\left(t\sqrt{\chi^2 - 1}\right)
\end{aligned} \tag{13}
$$

By combining Eqs. 8 and 9, we obtain the Quantum Chebyshev polynomials (Q-Chebyshev polynomials).

The q-exponential generating function of Chebyshev polynomials is:

$$
\begin{aligned}
&\sum_{n=0}^{\infty} [T_n]_q(\chi) \frac{t^n}{[n]_q!} \\
&= \frac{1}{2}\left(e_q\left(t\left(\chi - \sqrt{\chi^2-1}\right)\right) + e_q\left(t\left(\chi + \sqrt{\chi^2-1}\right)\right)\right)
\end{aligned} \tag{14}
$$

where

$$
[T_n]_q(\chi) = [n]_q \sum_{k=0}^{n} (-2)^k \frac{[n+k-1]_q!}{[n-k]_q![2k]_q!} (1-\chi)^k \tag{18}
$$

In this application, the nth coefficient of Eq. 15, when $k = n$, can be used, as follows

$$
[T_n]_q(\chi) = (\chi - 2)^n \left(\frac{q^n - 1}{q^{2n} - 1}\right) \tag{16}
$$

For one image block, the texture feature is given by Eq. (17).

$$[T_n]_q(\chi(k,l)) = \sum_{i=1}^{k}\sum_{j=1}^{l}(\chi(k,l)-2)^n\left(\frac{q^n-1}{q^{2n}-1}\right) \quad (17)$$

where (q) is the quantum number between 0, and 1, and (χ) is the pixel probability. The proposed image feature extraction model is defined in Eq. 17, which is based on Quantum Chebyshev polynomials (QCHPs) with the quantum number q. The proposed QChPs model extracts the image features based on the likelihood of each pixel probability as given in Algorithm 1. The feature extraction procedure begins by dividing the DCE-MRI slice into nonoverlapping blocks of size (4 × 4) pixels. Then, the texture features are extracted from every block. The proposed QChPs model preserves and improves morphological features in a high and low change gray-level respectively. Finally, every time phase of the breast DCE-MRI (pre and post-contrast) has a feature vector of 16 parameters (10, 2, and 4 features from kinetic, CNN, and QCHPs methods respectively). A total of 64 parameters are included in the feature vector, extracted from four-time phases of breast DCE-MRI (t_0, t_1, t_2, and t_3 respectively).

Algorithm 1: QCHPs

1: Initialization: I = Input image, set the quantum number q =0.8.
2: **For** each Input image I do
3: $[B_1, B_2, \ldots, B_n] \leftarrow I$ // Divide I into non-overlapped blocks of size (4×4) pixels.
4: **For** i=1 to n do
5: $T_i, \leftarrow I$ // Calculate $[T_n]_q(\chi)$. for each block (i) as defined in Eq. (17), where i denotes the i th block of (4×4) pixels.
6: $S_i \leftarrow T_i$ // For each texture feature T_i , the mean, variance, skewness, and kurtosis are computed.
7: **End For**
8: $QCHPs_I \leftarrow [S_1, S_2, S_3, \ldots. S_n]$ // Final QCHPs Features of all (n) blocks
9: **End For**

3.4 LSTM classifier

The LSTM was developed by Hochreiter and Schmidhuber to address the drawbacks of the artificial neural networks (ANNs) in sequential problems [15]. LSTM is capable of learning long-term dependencies and remembering information for prolonged periods of time as a default. The LSTM is used for classification of sequential and time-series data due to its ability to recognize image features across time by the connected memory blocks through its layers [17].

In this study, the LSTM includes seven layers, sequential input with 64 dimensions that comes from combined extracted features of breast DCE-MRI, 200-hidden units and 20% drop out. The LSTM network was also trained using the Adam optimization method, with the maximum epoch value set to 750 and the gradient threshold value set to 1.

4 Results and discussion

The experimental results show the effectiveness of the combined extracted features to classify the breast DCE-MRI into benign and malignant. In this study, 64 features were extracted by kinetic, CNN, and QCHPs methods from breast DCE-MRI sequences. The utilized dataset is adopted to evaluate the proposed model by preserving 70% of DCE-MRI slices for the training phase of CNN and LSTM, and 30% of the DCE-MRI slices are used to assess the final classification performance.

The utilized CNN was initialized experimentally by convolution layers, neurons, pooling layers, learning rate and kernel size. The proposed CNN included eight layers as summarized in Table 1. It is trained with the following parameters; the momentums are 0.9 with a learning rate of 0.0001, the maximum number of epochs is 30 with the minimum batch size of 64, and the maximum iteration number is 750. Figure 6 shows the training progress plot of the proposed CNN, and this indicates that the proposed CNN has a good performance in extracting DF from breast DCE-MRI sequences.

The performance of the combined kinetic, QCHPs, and DF features that were extracted from breast DCE-MRI sequences to differentiate malignant from benign lesions is evaluated by comparing the following metrics: the true positive (TP) rate and the true negative (TN). When the breast mass is classified as a benign, it is considered as a TP. When the breast mass is classified as a malignant, it is considered as a TN. A total of 600 unique breast lesions from 922 breast DCE-MRI sequences (mean age 50 ± 13 years; age range 25–75 years) were ultimately included in this study where 300 were benign and 300 were malignant. The median size of breast malignant lesions was 23 mm^3 (range, 10–65 mm^3), while for the benign lesions, it was 12 mm^3 (range, 5.5–30 mm^3). During experimentation, 70% of the dataset was used as the training part and the remaining 30% was used as unseen dataset for testing. These factors lead to the occurrence of random fluctuations in the intensity signal of DCE-MRI sequences. Therefore, the Gaussian filter and histogram normalization methods were implemented to enhance and normalize all DCE-MRI sequences respectively in the preprocessing stage.

The experimental results show that the extracted QCHPs features improved the efficacy of diagnosing the breast DCE-MRI sequences into malignant or benign breast lesions, when combined with kinetic and DF features and classified by LSTM model, as illustrated in Table 2. On the independent test dataset including both benign and malignant lesions, the trained LSTM model yielded an ACC and AUC values of 99.5% and 100% respectively in differentiating between benign and malignant breast lesions.

It is noted that the performance of diagnosing breast lesions was improved significantly when the kinetic features that are extracted by TIC analysis were combined with the proposed QCHPs features and DF features, and outperforms their performances when using them individually, as shown in Fig. 7. MATLAB R2021b was used for all statistical and computational studies (64-bit version) environment (The MathWorks, Natick, MA, USA).

Table 1 Proposed architecture of CNN

Layer name	Kernel filter	Kernel size	Feature map
Input layer		(98 × 98)	
Convolution layer 1	64	(3 × 3)	(98 × 98 × 64)
Pooling layer 1		(2 × 2)	(49 × 49 × 64)
Convolution layer 2	64	(3 × 3)	(49 × 49 × 64)
Pooling layer 2		(2 × 2)	(24 × 24 × 64)
Convolution layer 3	32	(7 × 7)	(24 × 24 × 32)
Pooling layer 3		(2 × 2)	(12 × 12 × 32)
Fully connected layer		(1 × 2)	(1 × 2)

There have been no studies examining the best timing of delayed post-contrast imaging for distinguishing benign from malignant suspicious lesions. Additionally, many medical institutions try to shorten timing of scan protocols for throughput and patient comfort. As a result, assessing too early may fail to sufficiently demonstrate washout in malignant lesions, whereas testing too late may overestimate washout kinetics in benign lesions [37]. Therefore, to determine the best post-contrast timing for discriminating malignant from benign breast lesions, independent sample *t*-test was used to choose the optimal post-contrast time for diagnosing malignance and benign breast lesions, as shown in Table 3. We conclude that the best post-contrast time for discriminating malignance from benign breast lesions (p-value < 0.0001) is at t_2 (5 min) after contrast injection.

Therefore, to determine the best post-contrast timing for discriminating malignant from benign breast lesions, independent sample *t*-test was used to choose the optimal post-contrast time for diagnosing malignance and benign breast lesions, as shown in Table 3. We conclude that the best post-contrast time for discriminating malignance from benign breast lesions (p-value < 0.0001), is at t_2 (5 min) after contrast injection.

4.1 Ablation study

The concept of ablation experiments to examine and demonstrate the validity of the proposed model of CNN by removing and replacing in order a convolutional layer, activation function, and pooling layer to figure out how these components impact the system's performance. To be more specific, the performance of the CNN model is evaluated by combining with the other feature sets of Kinetic and QCHP. An ablation analysis was performed using three experiments that involved changing the number of kernel filters that impact on the performance of the suggested network. Three subsets of kernel filters were tested in three convolutional layers respectively. These subsets are (32, 32 and 16), (64, 32 and 16), and (64, 64 and 16). The performance of the ablated models is summarized

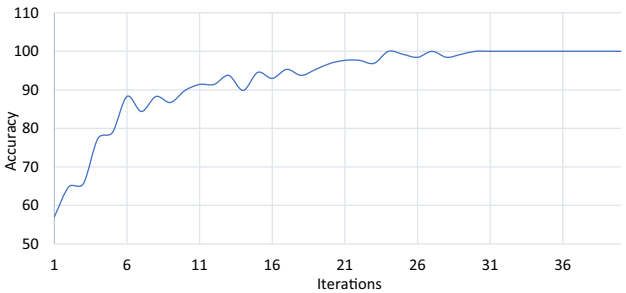

Fig. 6 The training plot of the proposed CNN

Table 2 Achieved results by the proposed QCHPs with and without kinetic and CNN features using LSTM classifier

Features	ACC 100%	TP 100%	TN 100%	Sensitivity 100%	Specificity 100%	AUC 100%
Kinetic features	83.3	85.0	81.7	82.3	84.5	79.0
QCHPs-Pre-contrast	84.2	81.6	86.6	85.9	82.5	81.0
QCHPs-Post-contrast 1	88.3	90.0	86.6	87.1	89.6	86.0
QCHPs-Post-contrast 2	93.2	94.0	92.3	92.5	93.9	95.0
QCHPs-Post-contrast 3	92.7	93.7	91.7	91.8	93.5	90.0
CNN-Pre-contrast	87.5	85.0	90.0	89.4	85.7	85.0
CNN-Post-contrast 1	93.6	94.0	93.3	93.4	93.7	95.0
CNN-Post-contrast 2	95.8	96.7	95.0	95.1	96.6	96.0
CNN-Post-contrast 3	94.2	95.0	93.3	93.4	95.0	95.0
Combined Features-Pre-contrast	89.2	88.3	90.0	89.8	88.5	87.0
Combined Features-Post-contrast 1	96.7	96.6	95.6	95.7	96.6	97.0
Combined Features-post-contrast 2	99.5	99.7	99.3	99.3	96.7	100
Combined Features-Post-contrast 3	97.5	98.3	96.7	96.7	98.3	98.0

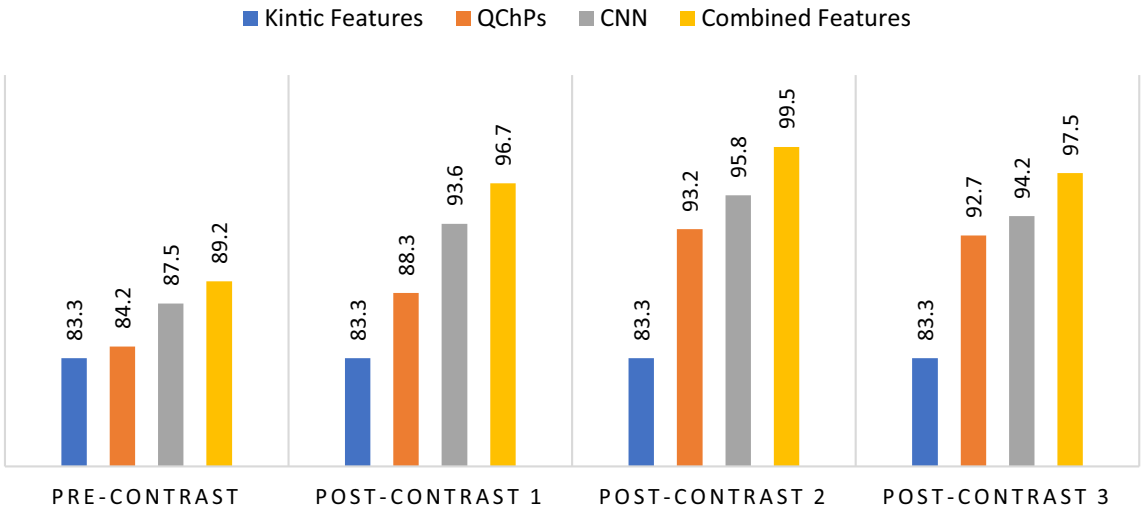

Fig. 7 Comparison of breast lesion classification of four DCE-MRI sequences by using Kinetic, QCHPs, CNN and combined features. Kinetic with QRP features

in Table 4. According to the achieved results by the three subset of kernel filter makes the system perform best.

4.2 Comparison with existing state-of-the art

To validate the effectiveness of the proposed method, Table 5 summarizes previous studies that investigated the diagnosis of breast DCE-MRI breast scans. Jing et al. [26] have used CNN with LSTM to classify DCE-MRI breast scans into malignant and benign, which was used to detect the possibility of breast cancer. The authors have achieved an AUC of 83% on 173 images. Other wok by Ji et al. [25] had used the combination of seven different features extracted from 1483 images. The achieved AUC was 89%. The use of morphological features with dynamic features was investigated in Fusco et al. [8]. On only 48 images, the reported achieved classification accuracy was improved to 91.70%. The CNN deep learning approaches have been further investigated to improve accuracy. It was reported that there is an urgent need to improve breast cancer detection by applying the CNN deep learning model. In Antropova et al. [4], the VGG Net with LSTM classifier has been applied for classifying 703 DCE-MRI breast images into malignant and benign cases, and the achieved AUC was 88%. Likewise, Hu et al. [18] have applied the VGG19 Net to classify 927 breast MRI into malignant and benign breast masses. The achieved detection accuracy was 87%.

Table 3 Comparison of post-contrast timings for differentiating benign from malignant tumors

Timings for delayed phase of kinetic curve	Median	*P*-value
t_0	0	0.0510
t_1	196 s. (3.26 min)	0.0160
t_2	310 s. (5.16 min)	0.0001
t_3	418 s. (6.96 min)	0.0040

Table 4 Ablation study

Experiment	Kernel filter (convolutional $layer_{1,\ 2,\ 3}$)	Accuracy (%)
Ablation study 1	32, 32 and 16	96.3
Ablation study 2	64, 32 and 16	96.7
Ablation study 3	64, 64 and 16	97.3
Proposed model	64, 64 and 32	99.5

Table 5 Comparisons of the proposed model to other breast DCE-MRI diagnosis methods

Refs.	Dataset	Classifier	Features	Accuracy 100%	AUC 100%
Fusco et al. [8]	48 (26 malignant and 22 benign	Decision tree Bayesian classifier	Morphological features Dynamic features	91.7	–
Ji et al. [25]	Tianjin Medical University Cancer Institute and Hospital, 1483 (987 malignant and 496 benign)	SVM	Radiomic features Size Shape Morphology Enhancement texture Kinetics Enhancement variance-kinetics	–	89
Yin et al. [46]	Shengjing Hospital, 156 (85 malignant and 71 benign)	–	Kinetic features Maximum slope of increase Signal intensity slop Initial percentage of enhancement Percentage of peak enhancement Early signal enhancement ratio Second enhancement percentage	82.05	–
Antropova et al. [4]	703 (482 malignant and 221 benign)	LSTM	VGG Net	–	88
Hu et al. [18]	927 (728 malignant and 199 benign)	SVM	VGG19 Net		87
Jing et al. [26]	173 (64 malignant and 109 benign)	LSTM	2D CNN LSTM	–	83

Table 5 (continued)

Refs.	Dataset	Classifier	Features	Accuracy 100%	AUC 100%
[12]	Duke University Hospital, 300 (150 malignant and 150 benign)	SVM	Kinetic features Signal intensity slop Maximum signal intensity Initial enhancement Percentage of peak enhancement Early signal enhancement ratio Second enhancement percentage Gradient QRPs features	97.4	100
Proposed	Duke University Hospital, 600 (300 malignant and 300 benign)	LSTM	Kinetic features Signal intensity slop Maximum signal intensity Initial enhancement Percentage of peak enhancement Early signal enhancement ratio Second enhancement percentage Gradient QCHPs features CNN	99.5	100

The proposed study was successful in detecting abnormalities that aid in the early detection of breast cancer, with a detection accuracy of 99.50%. The hybrid features of the DCE-MRI images were extracted from a publicly available dataset in this study. The proposed QCHPs model for textural extraction feature described the relationship of gray levels between neighboring pixels. The proposed mathematical method, which was thought to be important for breast cancer diagnosis, was able to extract features from the tumor region efficiently. The main limitation of this study was that it included mostly malignant lesions and a small number of benign lesions, which may make generalizing our findings to the entire spectrum of breast lesions difficult.

5 Conclusion

The early detection of breast cancer can help to reduce the mortality rate caused by the disease. The goal of this study was to detect the masses and to classify benign and malignant tissues in DCE-MRI. In this study, a new hybrid features extraction is proposed to boost the automatic identification of breast cancer by using three features extraction methods: Kinetic Features, CNN deep learning features, and new features extraction by proposed QCHPs to automatically detect breast cancer by using long short-term memory (LSTM) as the classifier. Future research will investigate other abnormalities such as carcinomas, masses, lumps, calcification, and asymmetry, all of which can indicate a potential breast cancer. Experimental results showed that the hybrid features extraction which was guided by a big publicly available dataset has achieved a detection accuracy of 99.50% in post-contrast 2, potentially. Future research will look into other abnormalities such as carcinomas, masses, lumps, calcification, and asymmetry, all of which can indicate a potential breast cancer.

Acknowledgements This study was supported by Al-Nahrain University, project (CMPMP-22-001), Iraq.

Author's contribution AMH was contributed to software, writing—original draft. HKA was contributed to data curation. NKNA-W was contributed to data curation, visualization. RWI was contributed to methodology, writing—review and editing. HAJ was contributed to software, validation. FM was contributed to investigation, conceptualization.

Data availability No data were used for the research described in the article.

Declarations

Conflict of interest The authors declare that they have no known competing financial interests or personal relationships that could have appeared to influence the work reported in this paper.

References

1. Al-Azawi RJ, Al-Saidi NM, Jalab HA, Kahtan H, Ibrahim RW (2021) Efficient classification of COVID-19 CT scans by using q-transform model for feature extraction. PeerJ Comput Sci 7:e553
2. MM, Al-Hashimi (2021) Trends in breast cancer incidence in Iraq during the period 2000–2019. Asian Pac J Cancer Prevent APJCP 22:3889
3. Alnafea MA (2017) Detection and diagnosis of breast diseases. Breast imaging. IntechOpen, London
4. Antropova N, Huynh B, Li H, Giger ML (2019) Breast lesion classification based on dynamic contrast-enhanced magnetic resonance images sequences with long short-term memory networks. J Med Imag (Bellingham) 6:011002
5. Chen HL, Zhou JQ, Chen Q, Deng YC (2021) Comparison of the sensitivity of mammography, ultrasound, magnetic resonance imaging and combinations of these imaging modalities for the detection of small ($\leq$ 2 cm) breast cancer. Medicine (Baltim) 100:e26531
6. Chen Y, Wang L, Luo R, Wang S, Wang H, Gao F, Wang D (2022) A deep learning model based on dynamic contrast-enhanced magnetic resonance imaging enables accurate prediction of benign and malignant breast lessons. Front Oncol 12:943415
7. Daimiel Naranjo I, Gibbs P, Reiner JS, Lo Gullo R, Thakur SB, Jochelson MS, Thakur N, Baltzer PAT, Helbich TH, Pinker K (2022) Breast lesion classification with multiparametric breast MRI using radiomics and machine learning: a comparison with radiologists & rsquo; Performance. Cancers 14:1743
8. Fusco R, di Marzo M, Sansone C, Sansone M, Petrillo A (2017) Breast DCE-MRI: lesion classification using dynamic and morphological features by means of a multiple classifier system. Eur Radiol Exp 1:10
9. Gilbert FJ, Pinker-Domenig K (2019) Diagnosis and staging of breast cancer: when and how to use mammography, tomosynthesis, ultrasound, contrast-enhanced mammography, and magnetic resonance imaging. In: Hodler J, Kubik-huch RA, von Schulthess GK (eds) Diseases of the chest, breast, heart and vessels 2019–2022: diagnostic and interventional imaging. Springer, Cham
10. Hasan A, Meziane F (2016) Automated screening of MRI brain scanning using grey level statistics. Comput Electr Eng 53:276–291
11. Hasan A, Meziane F, Aspin R, Jalab H (2016) Segmentation of brain tumors in MRI images using three-dimensional active contour without edge. Symmetry 8:132
12. Hasan AM, Al-Waely NK, Ajobouri HK, Ibrahim RW, Jalab HA, Meziane F (2023) A classification model of breast masses in DCE-MRI using kinetic curves features with quantum-Raina's polynomial based fusion. Biomed Signal Process Control 84:105002
13. Hasan AM, Jalab HA, Ibrahim RW, Meziane F, Al-Shamasneh AAR, Obaiys SJ (2020) MRI brain classification using the quantum entropy LBP and deep-learning-based features. Entropy 22:1033
14. Hasan AM, Meziane F, Aspin R, Jalab HA (2017) MRI brain scan classification using novel 3-D statistical features. In: Proceedings of the second international conference on internet of things, data and cloud computing. ACM, 1–5
15. Hasan AM, Qasim AF, Jalab HA, Ibrahim RW (2022) Breast cancer MRI classification based on fractional entropy image enhancement and deep feature extraction. Baghdad Sci J 20:0221–0221
16. Healthcare P (2022) dStream Breast 16ch coil. https://www.usa.philips.com/healthcare/product/HCNMRB106A/dstream-breast-16ch-coil-mr-coil
17. Hilal SR, Hasan HS, Hasan AM (2021) Magnetic resonance imaging breast scan classification based on texture features and long short-term memory model. NeuroQuantology 19:41
18. Hu Q, Whitney HM, Giger ML (2020) A deep learning methodology for improved breast cancer diagnosis using multiparametric MRI. Sci Rep 10:1–11
19. Hu Q, Whitney HM, Li H, Ji Y, Liu P, Giger ML (2021) Improved classification of benign and malignant breast lesions using deep feature maximum intensity projection MRI in breast cancer diagnosis using dynamic contrast-enhanced MRI. Radiol Artif Intell 3:e200159
20. Huang S, Qiu P, Zhang Y, Li J, Chen W, Chen B, Liang Z, Liang Z, Luo K, Huang B (2020) Reconstruction of the chest wall in locally advanced breast cancer with multi-disciplinary cooperation: a case report of mesh repair plus TRAM combined with DIEP chest wall reconstruction. Gland Surg 9:1048–1055
21. Ibrahim RW, Jalab HA, Karim FK, Alabdulkreem E, Ayub MN (2022) A medical image enhancement based on generalized class of fractional partial differential equations. Quant Imaging Med Surg 12:172
22. Jackson F (1910) On q-definite integrals. Quart J Pure Appl Math 41:193–203
23. Jafari SH, Saadatpour Z, Salmaninejad A, Momeni F, Mokhtari M, Nahand JS, Rahmati M, Mirzaei H, Kianmehr M (2018) Breast cancer diagnosis: imaging techniques and biochemical markers. J Cell Physiol 233:5200–5213
24. Jalab HA, Al-Shamasneh AAR, Shaiba H, Ibrahim RW, Baleanu D (2021) Fractional renyi entropy image enhancement for deep segmentation of kidney MRI. CMC-Comput Mater Contin 67:2061–2075
25. Ji Y, Li H, Edwards AV, Papaioannou J, Ma W, Liu P, Giger ML (2019) Independent validation of machine learning in diagnosing breast Cancer on magnetic resonance imaging within a single institution. Cancer Imaging 19:64
26. Jing X, Dorrius MD, Wielema M, Sijens PE, Oudkerk M, van Ooijen P (2022) Breast tumor identification in ultrafast MRI using temporal and spatial information. Cancers 14:2042
27. Krupa K, Bekiesińska-Figatowska M (2015) Artifacts in magnetic resonance imaging. Pol J Radiol 80:93–106
28. Lavini C, Buiter MS, Maas M (2013) Use of dynamic contrast enhanced time intensity curve shape analysis in MRI: theory and practice. Rep Med Imaging 6:71–82
29. Mayrhofer RM, Ng HP, Putti TC, Kuchel PW (2013) Magnetic resonance in the detection of breast cancers of different histological types. Magn Reson Insights 6:S10640

30. McDonald ES, Clark AS, Tchou J, Zhang P, Freedman GM (2016) Clinical diagnosis and management of breast cancer. J Nucl Med 57:9S-16S
31. Milosevic M, Jankovic D, Milenkovic A, Stojanov D (2018) Early diagnosis and detection of breast cancer. Technol Health Care 26:729–759
32. Mori N, Pineda FD, Tsuchiya K, Mugikura S, Takahashi S, Karczmar GS, Abe H (2018) Fast temporal resolution dynamic contrast-enhanced MRI: histogram analysis versus visual analysis for differentiating benign and malignant breast lesions. AJR Am J Roentgenol 211:933
33. Navaei Lavasani S, Mostaar A, Ashtiyani M (2018) Automatic prostate cancer segmentation using kinetic analysis in dynamic contrast-enhanced MRI. J biomed phys eng 8:107–116
34. Nievelstein RA, Quarles Van Ufford HM, Kwee TC, Bierings MB, Ludwig I, Beek FJ, de Klerk JM, Mali WP, de Bruin PW, Geleijns J (2012) Radiation exposure and mortality risk from CT and PET imaging of patients with malignant lymphoma. Eur Radiol 22:1946–1954
35. Nsaif GS, Abdallah AH, Ahmed NS, Alfatlawi WR (2018) Evaluation of estridiol and some antioxidant in breast cancer Iraqi women. Al-Nahrain J Sci 21:35–40
36. Onishi N, Sadinski M, Hughes MC, Ko ES, Gibbs P, Gallagher KM, Fung MM, Hunt TJ, Martinez DF, Shukla-Dave A (2020) Ultrafast dynamic contrast-enhanced breast MRI may generate prognostic imaging markers of breast cancer. Breast Cancer Res 22:1–13
37. Partridge SC, Stone KM, Strigel RM, Demartini WB, Peacock S, Lehman CD (2014) Breast DCE-MRI: influence of postcontrast timing on automated lesion kinetics assessments and discrimination of benign and malignant lesions. Acad Radiol 21:1195–1203
38. Peng Y, Cheng Z, Gong C, Zheng C, Zhang X, Wu Z, Yang Y, Yang X, Zheng J, Shen J (2022) Pretreatment DCE-MRI-based deep learning outperforms radiomics analysis in predicting pathologic complete response to neoadjuvant chemotherapy in breast cancer. Front Oncol 12:846775–846775
39. Piantadosi G, Marrone S, Fusco R, Sansone M, Sansone C (2018) Comprehensive computer-aided diagnosis for breast T1-weighted DCE-MRI through quantitative dynamical features and spatio-temporal local binary patterns. IET Comput Vision 12:1007–1017
40. Plewes DB, Kucharczyk W (2012) Physics of MRI: a primer. J Magn Reson Imaging 35:1038–1054
41. Saha A, Harowicz MR, Grimm LJ, Kim CE, Ghate SV, Walsh R, Mazurowski MA (2018) A machine learning approach to radiogenomics of breast cancer: a study of 922 subjects and 529 DCE-MRI features. Br J Cancer 119:508–516
42. Smith TB (2010) MRI artifacts and correction strategies. Imaging Med 2:445
43. Song J, Gu Y, Du T, Liu Q (2021) Analysis of quantitative and semi-quantitative parameters of DCE-MRI in differential diagnosis of benign and malignant cervical tumors. Am J Transl Res 13:12228–12234
44. Xiao J, Rahbar H, Hippe DS, Rendi MH, Parker EU, Shekar N, Hirano M, Cheung KJ, Partridge SC (2021) Dynamic contrast-enhanced breast MRI features correlate with invasive breast cancer angiogenesis. NPJ Breast Cancer 7:1–9
45. Yang S-N, Li F-J, Chen J-M, Zhang G, Liao Y-H, Huang T-C (2016) Kinetic curve type assessment for classification of breast lesions using dynamic contrast-enhanced MR imaging. PLoS ONE 11:e0152827
46. Yin J, Yang J, Jiang Z (2019) Classification of breast mass lesions on dynamic contrast-enhanced magnetic resonance imaging by a computer-assisted diagnosis system based on quantitative analysis. Oncol Lett 17:2623–2630
47. Zhang J, Saha A, Zhu Z, Mazurowski MA (2019) Hierarchical convolutional neural networks for segmentation of breast tumors in MRI with application to radiogenomics. IEEE Trans Med Imaging 38:435–447
48. Zhu J-J, Shen J, Zhang W, Wang F, Yuan M, Xu H, Yu T-F (2022) Quantitative texture analysis based on dynamic contrast enhanced MRI for differential diagnosis between primary thymic lymphoma from thymic carcinoma. Sci Rep 12:12629
49. Zhu Z, Albadawy E, Saha A, Zhang J, Harowicz MR, Mazurowski MA (2019) Deep learning for identifying radiogenomic associations in breast cancer. Comput Biol Med 109:85–90